

ELECTRONIC SUPPLEMENTARY INFORMATION

Eu(tta)₃DPPZ-based red organic light-emitting diodes: spin-coating vs vacuum-deposition

Kirill M. Kuznetsov,^a Makarii I. Kozlov,^a Andrey N. Aslandukov,^b Andrey A. Vashchenko,^c Alexey V. Medvedko,^a Egor V. Latipov,^a Alexander S. Goloveshkin,^d Dmitry M. Tsymbarenko,^a and Valentina V. Utochnikova^{a,e}

^aM.V. Lomonosov Moscow State University 1/3 Leninskiye Gory, Moscow, 119991, Russia

^bLaboratory of Crystallography, University of Bayreuth, 95440 Bayreuth, Germany

^cP.N. Lebedev Physical Institute, Leninsky prosp. 53, Moscow, 119992, Russia

^dA.N. Nesmeyanov Institute of Organoelement Compounds, Vavilova St. 28, Moscow, 119334, Russia

^eEVOLED Ltd, 1A-24 Puškina iela, Riga LV-1050, Latvia

Contents

Experimental section	2
TGA data and IR-spectroscopy	5
¹ H NMR spectroscopy	6
Crystal structure of Eu(tta) ₃ DPPZ·MeCN	7
Photo- and electroluminescent properties of thin films	8
Comparison of spin-coated and vapor-deposited OLEDs.....	10
Morphology of deposited layers in OLED heterostructure	11

Experimental section

Material and methods

All solvents and chemicals were purchased from commercial sources.

Synthesis of Eu(tta)₃DPPZ. A solution of 1 mmol of EuCl₃·6H₂O in 20 ml of ethanol was added to a mixture of Htta (3 mmol), Et₃N (3 mmol) in 20 ml of ethanol, then a solution of DPPZ (1 mmol) in 30 ml of ethanol was added, and the precipitation was observed. The reaction mixture was stirred for 2h, then the precipitate was filtered off, washed with cold ethanol, and dried in air.

X-ray powder diffraction (XRD) The powder patterns were measured on Bruker D8 Advance diffractometer with LynxEye detector and Ni filter monochromator, $\lambda(\text{CuK}\alpha) = 1.5416 \text{ \AA}$, θ/θ scan from 5° to 50°, step size 0.020°. The measurement was performed in reflection mode, the compounds were deposited on silicon zero-background holder. The refinement of the powder patterns was performed in TOPAS 5.0 software [1].

Single crystals of C₄₄H₂₅EuF₉N₅O₆S₃ were grown from acetonitrile. A suitable crystal was selected and mounted on a 'Bruker APEX-II CCD' diffractometer. The crystal was kept at 298 K during data collection. Using Olex2 [2], the structure was solved with the XS [3] structure solution program using Direct Methods and refined with the XL [3] refinement package using Least Squares minimization.

¹H NMR spectra were recorded at 25 °C using an Agilent 400 MR spectrometer with an operating frequency of 400.130 MHz. Chemical shifts are reported in ppm relative to Me₄Si (1H). **Thermal analysis** was carried out on a thermoanalyzer STA 409 PC Luxx (NETZSCH, Germany) in the temperature range of 20–1000 °C in air and at a heating rate of 10° min⁻¹. The evolved gases were simultaneously monitored during the TA experiment using a coupled QMS 403C Aeolos quadrupole mass spectrometer (NETZSCH, Germany). The mass spectra were registered for the species with the following m/z values: 18 (corresponding to H₂O), 44 (corresponding to CO₂) and 46 (corresponding to C₂H₅OH). **IR spectra** in the ATR mode were recorded on a spectrometer FTIR Nicolet iS50 in the region of 500–4000 cm⁻¹.

Emission and excitation spectra of thin films were recorded using a FluoroMax Plus spectrophotometer upon excitation with a xenon lamp. Luminescence lifetime measurements were recorded and detected on the same system. All luminescence decays proved to be perfect single-exponential functions. Photoluminescence quantum yields in

the visible range were determined with the FluoroMax Plus spectrophotometer at room temperature upon excitation into ligand states according to an absolute method using an integration sphere. The modified de Mello *et al.* [4] method requires the measurement of L_a , the integrated intensity of light exiting the sphere when the empty cuvette is illuminated at the excitation wavelength (Rayleigh scattering band); L_c , the same integrated intensity at the excitation wavelength when the sample is introduced into the sphere; E_a the integrated intensity of the entire emission spectrum of the empty cuvette; and E_c the integrated intensity of the entire emission spectrum of the cuvette with the sample. The absolute quantum yield is then given by:

$$PLQY = \frac{E_c - E_a}{L_a - L_c} \times 100\%$$

Composite films preparation. Composite films of $\text{Eu}(\text{tta})_3\text{DPPZ}$ (wt%):CBP, where wt = 1%, 2%, 5%, 10%, 25%, 50%, 75%, 100%, were deposited from a 200 μL THF solution of the complex and the host (5 g L^{-1} concentration) at 1500 rpm for 1 min and heated at 80 °C for 20 min.

Atomic force microscopy

The atomic force microscopy (AFM) was performed on NTEGRA Aura (NT-MDT). The AFM instrument was operated in tapping mode using silicon probes Micro-Science N15 (tip radius < 10 nm). All AFM images were taken in air at room temperature.

Absorption spectra of thin films

The absorption spectra of the thin films were recorded using an Ocean Optics HR4000CG-UV-NIR spectrometer in the measurement range between 290 nm and 800 nm.

OLED fabrication

Prepatterned indium tin oxide coating with 15 Ohm per sq on the glass substrates (Lumtec Corp.) were used as anodes. The substrates were sequentially washed in an ultrasonic bath with NaOH solution (30 min), distilled water (10 min), and 2-propanol (10 min) and then dried under a flow of N_2 . All the spin-coating deposition processes were performed under ambient air conditions. A 50 nm-thick PEDOT:PSS (poly(3,4-ethylenedioxythiophene):poly(styrenesulfonate), Lumtec Corp.) hole-injection layer was deposited by pouring 200 μl of the solution onto the substrate, followed by rotation for 1 min at 2000 rpm. The obtained film was dried at 100 °C for 20 min. A 20 nm-thick hole-transporting poly-TPD (Ossila) was spin-coated from chlorobenzene ($c = 5 \text{ g L}^{-1}$) at 2000 rpm for 1 min and then dried at 100 °C for 10 min. Finally, emission layers were spin-coated from 200 μl tetrahydrofuran solution ($c = 5 \text{ g L}^{-1}$ for $\text{Eu}(\text{tta})_3\text{DPPZ}$ (wt%):CBP,

where wt = 2%, 25%, 50%, 100%, and c = 10 g L⁻¹ for Eu(tta)₃DPPZ (25%):CBP for the second experiment) at 1500 rpm for 1 min or thermally evaporated (Univex-300, LeyboldHeraeus) under a pressure of below 10⁻⁵ mbar.

After deposition the substrates were transferred into an argon glove box where solution-deposited emission layers were dried at 80 °C for 20 minutes. The ~20 nm-thick electron-transporting layer TPBi (Lumtec Corp.) was thermally evaporated (Univex-300, LeyboldHeraeus) followed by an ~1 nm-thick LiF layer and a >100 nm-thick aluminum layer as the cathode under a pressure of below 10⁻⁵ mbar. The thicknesses of the layers were controlled by a quartz microbalance resonator pregraded by atomic force microscopy. Measurements of the OLED characteristics were performed in the argon glove box. Electroluminescence spectra were obtained using an Ocean Optics Maya 2000 Pro CCD spectro- meter sensitive within 200–1100 nm. I–V curves were measured using two DT 838 digital multimeters. The luminance was measured using a TKA-PKM luminance meter (TKA Instruments).

Synthesis of Eu(tta)₃DPPZ. A solution of 1 mmol of EuCl₃·6H₂O in 20 ml of ethanol was added to a mixture of Htta (3 mmol), Et₃N (3 mmol) in 20 ml of ethanol, then a solution of DPPZ (1 mmol) in 30 ml of ethanol was added, and the precipitation was observed. The reaction mixture was stirred for 2h, then the precipitate was filtered off, washed with cold ethanol, and dried in air.

1. Bruker, *TOPAS 5.0 User Manual*, Bruker AXS GmbH, Karlsruhe, Germany, 2014.
2. Dolomanov, O.V., Bourhis, L.J., Gildea, R.J, Howard, J.A.K. & Puschmann, H. 2009, *J. Appl. Cryst.* 42, 339-341.
3. Sheldrick, G.M. 2008. *Acta Cryst.* A64, 112-122.
4. J. C. De Mello, H. F. Wittmann and R. H. Friend, *Adv. Mater.*, 1997, 9, 230–232.

TGA data and IR-spectroscopy

The TGA data of $\text{Eu}(\text{tta})_3\text{DPPZ}\cdot\text{EtOH}$ (Fig. S1a) revealed that its decomposition occurs in three stages: first, in the range of 120–130°C molecule of EtOH is eliminated, which results in the formation of $\text{Eu}(\text{tta})_3\text{DPPZ}$. Thermal decomposition of the complex begins in the range of 280–290°C which occurs in two stages; the final weight loss corresponds to the formation of a mixture of Eu_2O_3 and EuOF from $\text{Eu}(\text{tta})_3\text{DPPZ}$, which witnesses the correctness of the ascribed composition.

The presence of coordinated solvent molecules was confirmed by IR-spectroscopy. In the spectrum of $\text{Eu}(\text{tta})_3\text{DPPZ}\cdot\text{EtOH}$ (Fig.S1b), low intensity bands at 3100–2800 cm^{-1} are observed, corresponding to the aromatic and methane C–H vibrations of DPPZ and tta^- , bands at 1750–1150 cm^{-1} , corresponding to C=O vibrations in tta^- , and bands at 850–515 cm^{-1} corresponding to the C–F vibrations, which are also present in the anionic ligand. The presence of the low intense broad band at ca. 3400 cm^{-1} , corresponding to the vibrations of the O–H bond, witnesses the presence of coordinated ethanol molecule.

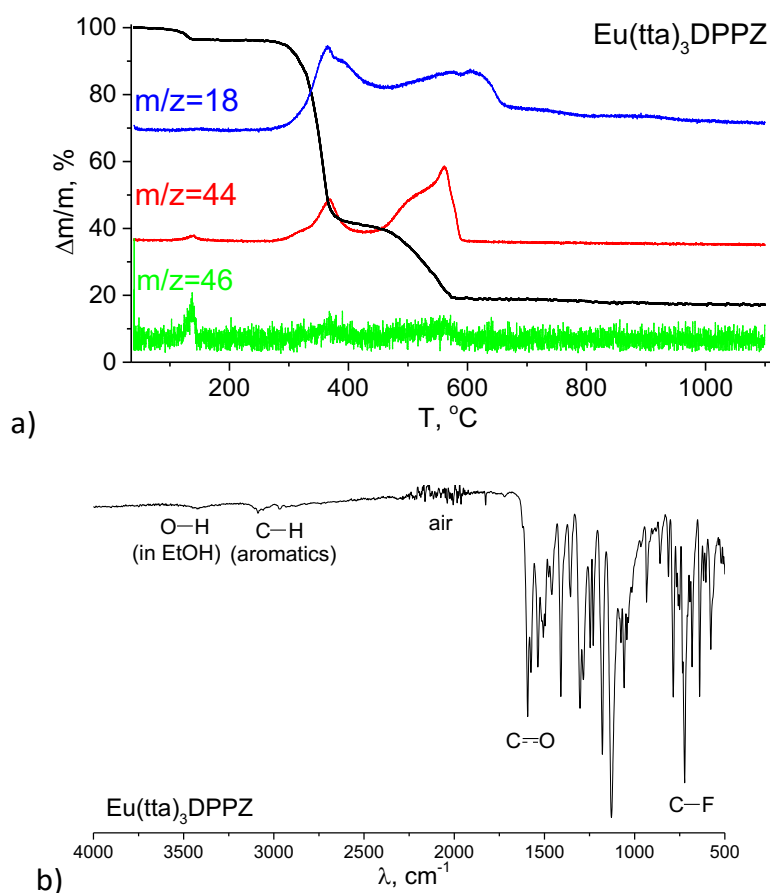


Fig.S1. a) TGA curve of $\text{Eu}(\text{tta})_3\text{DPPZ}\cdot\text{EtOH}$. Normalized ionic currents are shown in blue ($m/z = 18$), red ($m/z = 44$), and green ($m/z = 46$). b) IR-spectrum of $\text{Eu}(\text{tta})_3\text{DPPZ}\cdot\text{EtOH}$.

^1H NMR spectroscopy

In order to confirm the ratio of the neutral ligand DPPZ and the anionic ligand tta^- in compound, ^1H NMR spectrum of the $\text{Eu}(\text{tta})_3\text{DPPZ}$ was studied. Owing to the effect of a paramagnetic Eu^{3+} ion, broadening and a shift of proton signals are observed in the ^1H NMR spectrum. Therefore, for the correct analysis the obtained spectrum was compared to the spectrum of DPPZ (Fig. S2). The comparison of ^1H NMR spectra shows that total integrated intensity is equal to three anionic ligands per each neutral ligand. This confirms the composition of $\text{Eu}(\text{tta})_3\text{DPPZ}$.

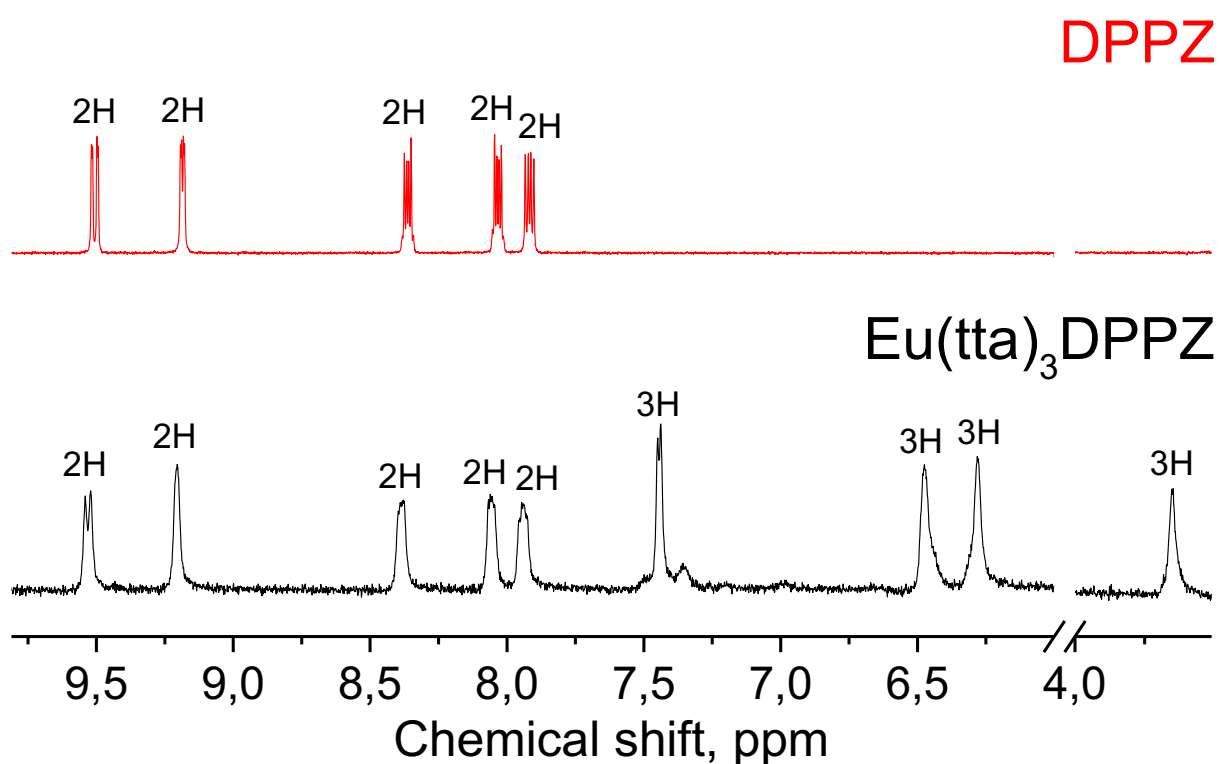


Fig.S2. The ^1H NMR spectra of the $\text{Eu}(\text{tta})_3\text{DPPZ}$ and DPPZ in DMSO-d_6 solution.

Crystal structure of Eu(tta)₃DPPZ·MeCN

Crystal Data for C₄₄H₂₅EuF₉N₅O₆S₃ (*M* = 1138.83 g/mol): monoclinic, space group P2₁/n (no. 14), *a* = 10.7467(3) Å, *b* = 20.2118(6) Å, *c* = 21.5322(7) Å, β = 101.444(2)°, *V* = 4584.0(2) Å³, *Z* = 4, *T* = 296.15 K, μ(MoKα) = 1.595 mm⁻¹, *D*_{calc} = 1.650 g/cm³, 55622 reflections measured (3.86° ≤ 2θ ≤ 56.56°), 11382 unique (*R*_{int} = 0.0688, *R*_{sigma} = 0.0664) which were used in all calculations. The final *R*₁ was 0.0906 (>2σ(*I*)) and *wR*₂ was 0.1869 (all data). The structure parameters were deposited with the Cambridge Structural Database (CCDC 2072867) deposit@ccdc.cam.ac.uk or http://www.ccdc.cam.ac.uk/data_request/cif.

Table S1. Cell parameters obtained from single-crystal and powder X-ray diffraction

	Single-crystal	Powder
Space group	P21/n	P21/n
<i>a</i> , Å	10.7467(3)	10.7364(12)
<i>b</i> , Å	20.2118(6)	20.2453(16)
<i>c</i> , Å	21.5322(7)	21.381(2)
β, °	101.444(2)°	102.038(8)
<i>V</i> , Å ³	4584.0(2)	4545.2(8)

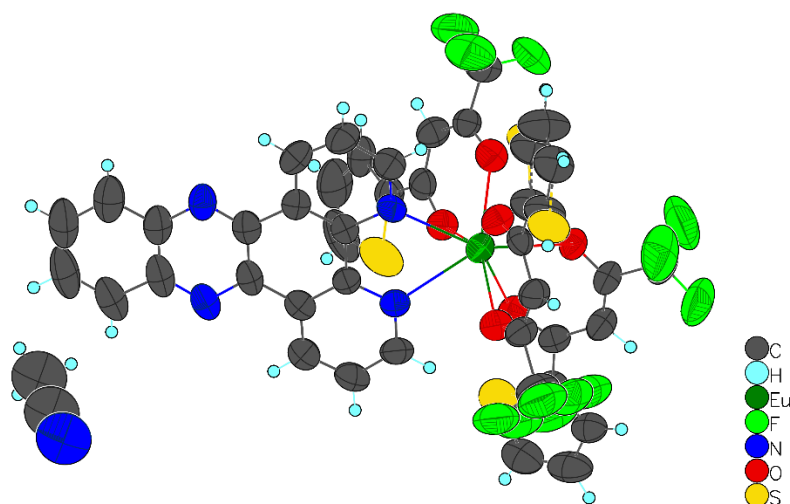


Fig.S3. The independent part of the unit cell of [Eu(tta)₃DPPZ]·MeCN. Atoms are represented by thermal displacement ellipsoids (ρ = 50%).

Photo- and electroluminescent properties of thin films

We studied photoluminescent properties of composite films, in order to increase the hole mobility, $\text{Eu}(\text{tta})_3\text{DPPZ}$ was doped into CBP. Thus, composite films of $\text{Eu}(\text{tta})_3\text{DPPZ}$ (x wt%):CBP, where $x = 1\%, 2\%, 5\%, 10\%, 25\%, 50\%, 75\%, 100\%$, were deposited on quartz glasses from a 200 μL THF solution of the complex and the host (5 g L^{-1} concentration) at 1500 rpm for 1 min and heated at 80 $^\circ\text{C}$ for 20 min.

To understand the reason of low quantum yield and lifetime of $\text{Eu}(\text{tta})_3\text{DPPZ}$, the radiative lifetime (τ_{rad}) and internal quantum yield ($Q^{\text{Ln}}_{\text{Ln}}$) were also calculated (Table 1). The low quantum yield results both from inefficient sensitization ($\eta_{L \rightarrow \text{Eu}}=9\%$) and quenching ($Q^{\text{Ln}}_{\text{Ln}}=8\%$). Both factors result from the low triplet state energy of DPPZ ($T_1=16400 \text{ cm}^{-1}$), which lies below the resonance level of Eu^{3+} ($E(^5\text{D}_0)=17200 \text{ cm}^{-1}$) and causes inefficient direct and efficient back energy transfer.

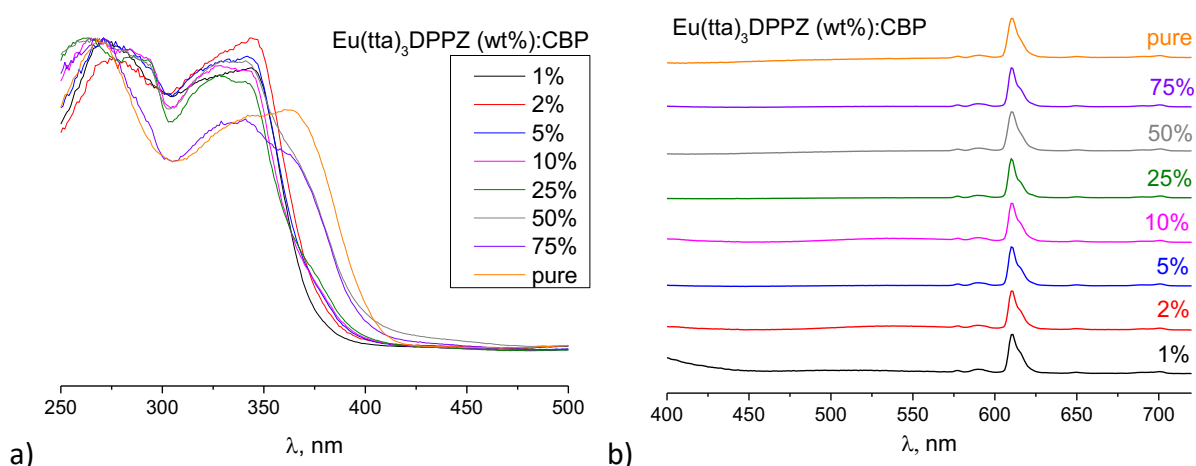


Fig.S4. a) Excitation and b) luminescence spectra of composite thin films.

After that solution-processed OLEDs were obtained with composite films used as EML. PEDOT:PSS was used as a hole-injection layer, which is the most widespread material for solution deposition. Poly-TPD was used as a hole-transport layer because it is resistant to many solvents after thermal treatment, unlike other hole-transport layer materials. TPBi was chosen as the electron transport layer, as it ensures balanced electron and hole currents when used in the heterostructure with poly-TPD.

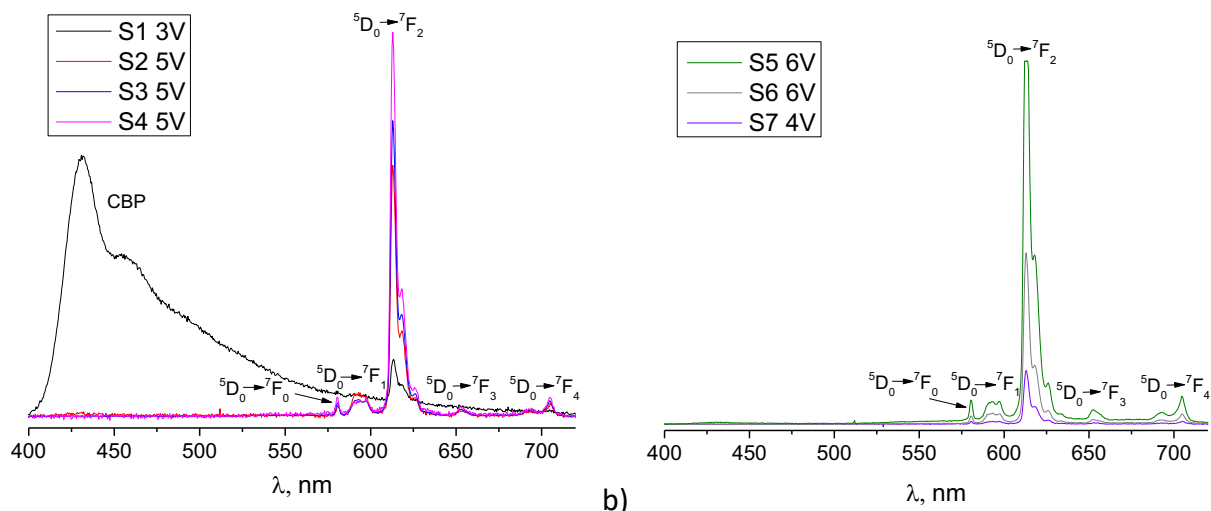


Fig.S5. Electroluminescence spectra of a) OLEDs S1-S4 and b) OLEDs S5-S7.

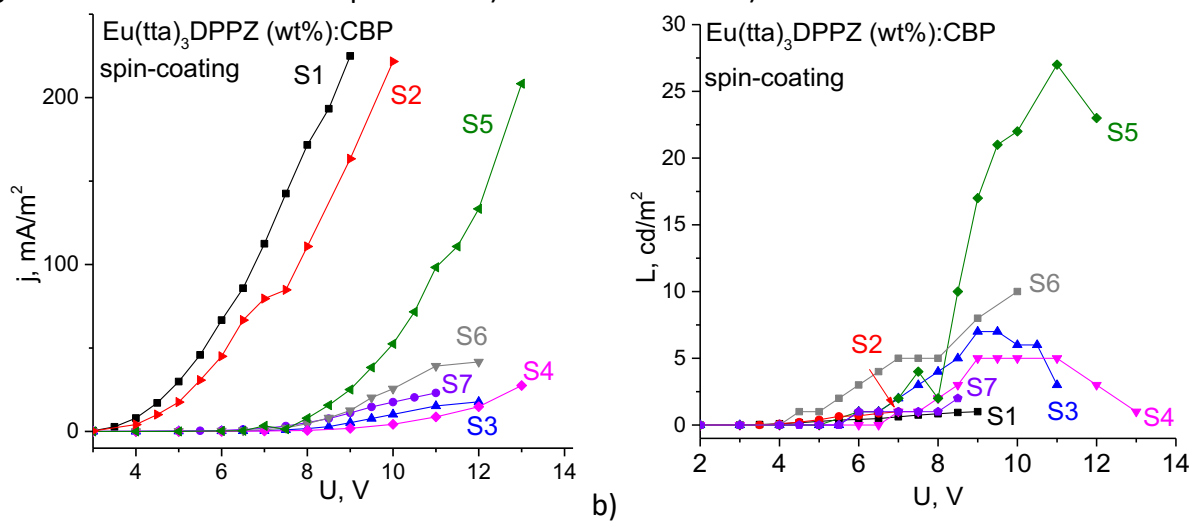


Fig.S6. a) I-V curves and b) L-V curves of OLEDs S1-S7.

Comparison of spin-coated and vapor-deposited OLEDs

Degradation from time was measured for spin-coated and vapor-deposited OLEDs. It was found out that they degraded almost identically.

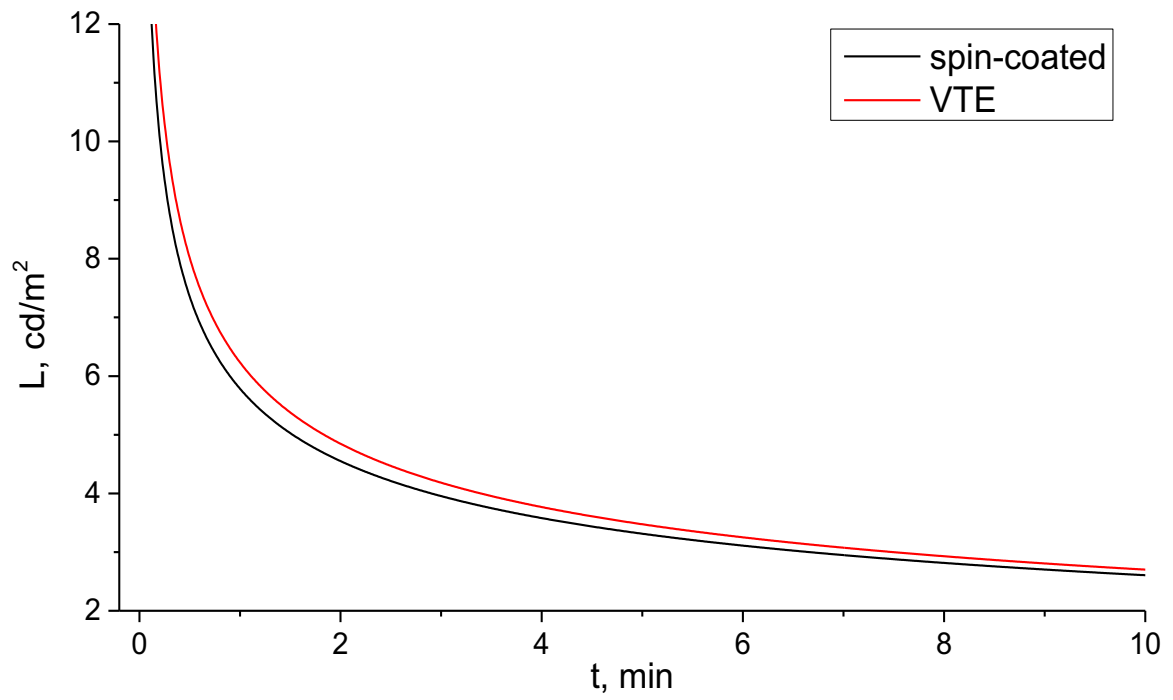


Fig.S8. Degradation from time of OLEDs.

Morphology of deposited layers in OLED heterostructure

Before fabricating OLED, we measured thickness of each layer in heterostructure. Each layer was deposited consistently which was done to normalize the resulting thickness of deposited layer. Therefore, top layer thickness and root mean square (RMS) of roughness values were obtained for each layer (Table S2). Morphology of every obtained film demonstrated rather high smoothness (Fig. S8).

Table S2. Morphology and thickness of deposited layers in OLED heterostructure.

No	Heterostructure	Total thickness, nm	Top layer thickness, nm	RMS, 5x5	RMS, 10x10
1	ITO	0	-	-	-
2	ITO/PEDOT:PSS	43	43	2	2
3	ITO/PEDOT:PSS/poly-TPD	57	15	-	1
4	ITO/PEDOT:PSS/poly-TPD/Eu(tta) ₃ DPPZ (VTE)	80	23	1	1
5	ITO/PEDOT:PSS/poly-TPD/Eu(tta) ₃ DPPZ (spin-coating, 5 g L ⁻¹ , 1500 rpm)	66	9	2	2
6	ITO/PEDOT:PSS/poly-TPD/Eu(tta) ₃ DPPZ (spin-coating, 10 g L ⁻¹ , 1500 rpm)	85	27	1	1
7	ITO/PEDOT:PSS/poly-TPD/Eu(tta) ₃ DPPZ:CBP (1:3) (spin-coating, 5 g L ⁻¹ , 1500 rpm)	73	14	-	-
8	ITO/Eu(tta) ₃ DPPZ (VTE)	23	23	3	-
9	ITO/PEDOT:PSS/poly-TPD/Eu(tta) ₃ DPPZ:CBP (1:3) (spin-coating)	112	54	1	
10	ITO/PEDOT:PSS/poly-TPD/Eu(tta) ₃ DPPZ:CBP (1:3) (VTE)	111	53	1	

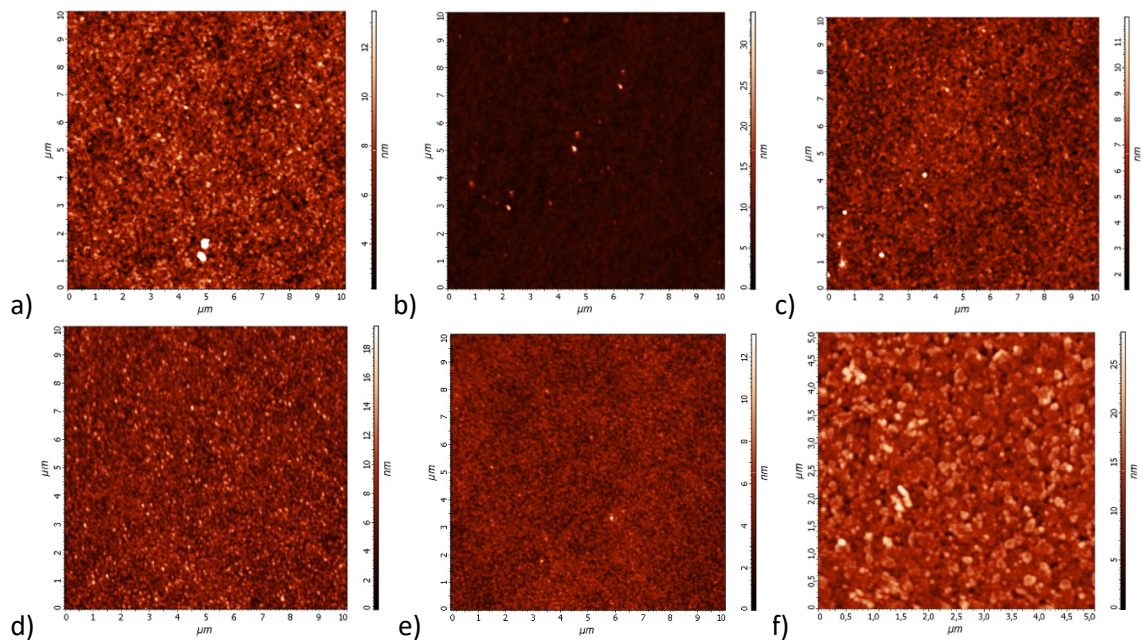


Fig.S9. 10×10 μm² AFM scans of a) ITO/PEDOT:PSS, b) ITO/PEDOT:PSS/poly-TPD, c) ITO/PEDOT:PSS/poly-TPD/Eu(tta)₃DPPZ (VTE), d) ITO/PEDOT:PSS/poly-TPD/Eu(tta)₃DPPZ (spin-coating, 5 g L⁻¹, 1500 rpm), e) ITO/PEDOT:PSS/poly-TPD/Eu(tta)₃DPPZ (spin-coating, 10 g L⁻¹, 1500 rpm) heterostructure, f) 5×5 μm² AFM scans of ITO/Eu(tta)₃DPPZ (VTE).